ELSEVIER

Available online at www.sciencedirect.com

ScienceDirect

Applied Mathematical Modelling 31 (2007) 1847–1864

APPLIED MATHEMATICAL MODELLING

www.elsevier.com/locate/apm

# A non-Newtonian fluid flow model for blood flow through a catheterized artery—Steady flow

D.S. Sankar [a,*], K. Hemalatha [b]

[a] *Department of Mathematics, Crescent Engineering College, Vandalur, Chennai 600 048, Tamil Nadu, India*
[b] *Department of Mathematics, Anna University, Chennai 600 025, Tamil Nadu, India*

Received 1 March 2005; received in revised form 1 May 2006; accepted 27 June 2006
Available online 17 August 2006

**Abstract**

In this paper the effects catheterization and non-Newtonian nature of blood in small arteries of diameter less than 100 μm, on velocity, flow resistance and wall shear stress are analyzed mathematically by modeling blood as a Herschel–Bulkley fluid with parameters $n$ and $\theta$ and the artery and catheter by coaxial rigid circular cylinders. The influence of the catheter radius and the yield stress of the fluid on the yield plane locations, velocity distributions, flow rate, wall shear stress and frictional resistance are investigated assuming the flow to be steady. It is shown that the velocity decreases as the yield stress increases for given values of other parameters. The frictional resistance as well as the wall shear stress increases with increasing yield stress, whereas the frictional resistance increases and the wall shear stress decreases with increasing catheter radius ratio $k$ (catheter radius to vessel radius). For the range of catheter radius ratio 0.3–0.6, in smaller arteries where blood is modeled by Herschel–Bulkley fluid with yield stress $\theta = 0.1$, the resistance increases by a factor 3.98–21.12 for $n = 0.95$ and by a factor 4.35–25.09 for $n = 1.05$. When $\theta = 0.3$, these factors are 7.47–124.6 when $n = 0.95$ and 8.97–247.76 when $n = 1.05$.


*Keywords:* Steady flow; Catheterized artery; Herschel–Bulkley fluid; Yield planes; Resistance to flow

## 1. Introduction

In recent times with the evolution of coronary balloon angioplasty, there has been considerable increase in the use of catheters of various sizes. These include the guiding catheter whose tip is positioned in the coronary ostium through which the angioplasty catheter over the small guidewire is advanced, and also the doppler catheter if used in the procedure with the tip positioned proximal to the coronary lesion. The insertion of a catheter in an artery will increase the frictional resistance to flow through the artery and hence alter the flow field and modify the pressure distribution. The mean pressure gradient is the mean pressure difference between the coronary ostium and just distal to the stenosis and thus includes the proximal vessel or vessels

* Corresponding author. Tel.: +91 44 22751375x393; fax: +91 44 22750520; mobile: +91 9444122916.
*E-mail address:* sankar_ds@yahoo.co.in (D.S. Sankar).

0307-904X/$ - see front matter 
doi:10.1016/j.apm.2006.06.009

**Nomenclature**

| | |
|---|---|
| $k$ | dimensionless catheter radius |
| $n$ | Herschel–Bulkley fluid's parameter |
| $\bar{p}$ | pressure |
| $p_s$ | dimensionless steady state pressure gradient |
| $\bar{p}_0$ | absolute magnitude of a typical pressure gradient |
| $Q_s$ | dimensionless steady flow rate |
| $\bar{R}$ | radius of the artery |
| $\bar{r}$ | radial distance |
| $r$ | dimensionless radial distance |
| $\bar{u}$ | axial velocity |
| $u$ | dimensionless axial velocity |
| $\bar{z}$ | axial distance |

*Greek letters*

| | |
|---|---|
| $\Lambda$ | dimensionless frictional resistance to flow |
| $\beta_s$ | width of the plug flow region in steady flow |
| $\lambda$ | radial plane at which the shear stress is zero |
| $\lambda_1$ | first yield plane location (dimensionless) |
| $\lambda_2$ | second yield plane location (dimensionless) |
| $\bar{\eta}$ | Herschel–Bulkley fluid's viscosity |
| $\bar{\tau}$ | shear stress |
| $\tau$ | dimensionless shear stress |
| $\bar{\tau}_y$ | yield stress |
| $\theta$ | dimensionless yield stress |

*Subscripts*

| | |
|---|---|
| p | plug flow value (used for $u$) |
| s | steady flow value (used for $p$, $Q$ and $\beta$) |
| w | value at the wall (used for $\tau$) |

*Superscripts*

| | |
|---|---|
| $+$ | the region $k \leqslant r \leqslant \lambda_1$ (used for $u$) |
| $++$ | the region $\lambda_2 \leqslant r \leqslant 1$ (used for $u$) |

where bifurcations were present. This is often referred to as the translesional pressure gradient. Even smaller coronary infusion catheters have been used to measure the mean pressure gradient [1]. Of particular interest, the relatively large mean translesional pressure gradients that have been reported, of the order $\Delta p = 50$ mm Hg for basal flow before coronary angioplasty [2]. This value is about 50% of the 100 mm Hg time averaged overall pressure drop across the coronary arteries and veins. After increasing the minimal lesion cross-sectional area by balloon angioplasty, the mean translesional pressure gradients were reduced to the range 10–15 mm Hg. The clinical investigators realize the limitations of the translesional pressure gradient measurements because of the obstruction by the angioplasty catheter [2,3].

Therefore the pressure or pressure gradient recorded by a transducer attached to the catheter will differ from that of an uncatheterized artery and it is essential to know the catheter induced error. Even very small angioplasty guidewire leads to sizable increase in flow resistance. For an angioplasty guidewire, over the catheter radius ratio (catheter radius to coronary vessel radius) from 0.3 to 0.7 (which is currently used clinically), even for Newtonian fluid, the flow resistance increased by a large factor of 3–33 for concentric configurations

[1]. For smaller infusion catheter, the flow resistance increase is less, although still appreciable. Therefore it is meaningful to study the increase in flow resistance due to catheterization.

Back and Denton [4] obtained the estimates of wall shear stress and discussed its clinical importance in coronary angioplasty. In routine clinical studies and animal experiments, the measurement of arterial blood pressure/pressure gradient and flow velocity/flow rate is usually achieved by the use of an appropriate catheter-tool device (such as catheter transducer system or a catheter tip flow meter) in the desired part of the arterial network. Catheters are also being used in diagnostic techniques (e.g., X-ray angiography, intravascular ultrasound) as well as in the treatment procedures (e.g. balloon angioplasty) of various arterial diseases. The direct measurement of arterial pressure or pressure gradient is frequently achieved by the use of a small strain gauge pressure transducer which is coupled to a flexible membrane – a sensing device – on the wall of the catheter. Back [1] and Back et al. [5] studied the important hemodynamic characteristics like the wall shear stress, pressure drop and frictional resistance in catheterized coronary arteries under normal as well as the pathological situation of a stenosis present. In all the above investigations, blood has been treated as a Newtonian fluid. But it is well known that, blood being suspension of cells, behaves like a non-Newtonian fluid at low shear rates and during its flow through narrow blood vessels. Aroesty and Gross [6] have studied the pulsatile flow of blood in small blood vessels and Chaturani and Ponnalagar Samy [7] extended this theory to study pulsatile flow of blood in stenosed arteries, modeling blood by Casson fluid.

The effect of catheterization on various flow characteristics in a curved artery was studied by Karahalios [8] and Jayaraman and Tiwari [9] treating blood as a Newtonian fluid. Dash et al. [10] studied the changed flow pattern in narrow artery when a catheter is inserted into it and estimated the increase in the friction in the artery due to catheterization using Casson fluid model for blood. Dash et al. [11] have studied the steady flow of Newtonian fluid through a catheterized curved artery with stenosis using toroidal coordinate system. Daripa and Dash [12] have analyzed the numerical study of pulsatile blood flow in an eccentric catheterized artery using a fast algorithm treating blood as a Newtonian fluid. Vajravelu et al. [13] have analyzed the peristaltic transport of Herschel–Bulkley fluid in an inclined tube. Sankar and Hemalatha [14] have studied the pulsatile flow of Herschel–Bulkley fluid through catheterized arteries using perturbation method. In this paper, we study the steady flow of Herschel–Bulkley fluid through catheterized arteries.

Scot Blair and Spanner [15] reported that blood obeys Casson equation only in the limited range, except at very high and very low shear rate and that there is no difference between the Casson plots and the Herschel–Bulkley plots of experimental data over the range where the Casson plot is valid. It is observed that the Casson fluid model can be used for moderate shear rates $\gamma < 10/s$ in smaller diameter tubes whereas the Herschel–Bulkley fluid model can be used at still lower shear rate of flow in very narrow arteries where the yield stress is high [15,16]. Since the Herschel–Bulkley equation contains one more parameter than the Casson equation does, it would be expected that more detailed information about blood properties can be obtained by the use of the Herschel–Bulkley equation. Furthermore, the Herschel–Bulkley equation is reduced to the mathematical models which describes the behaviour of Newtonian fluid, Bingham fluid and power law fluid by taking appropriate values of the parameters.

It has been pointed out both by Iida [17] and Scott Blair [18] that Herschel–Bulkley fluid model is more appropriate and more general for blood flow even though it is possible to model the same flow both by Casson fluid as well as by Herschel–Bulkley fluid over the range where both models are valid. Scott Blair [18] has pointed out that the residual variation which is the sum of the squares of the deviations of the observed values of stress from the estimated values was lowest for Herschel–Bulkley fluid compared to Casson fluid model, but the effort in calculations for Herschel–Bulkley fluid is more. Iida [17] reported that the velocity profile in the arterioles having diameter less than 100 μm are generally explained fairly by the two models. However, velocity profiles in the arterioles whose diameters are less than 65 μm does not conform to the Casson model but can still be explained by Herschel–Bulkley model.

Therefore in this paper we study the effect of catheterization on various physiologically important flow characteristics (i.e. pressure drop, wall shear stress and impedance) for blood flow in a narrow artery of diameter less than 100 μm, by modeling blood as a Herschel–Bulkley fluid and the artery and the catheter as coaxial rigid tubes. Section 2 deals with the general mathematical formulation of the problem in which equations of motion and the appropriate constitutive equations for Herschel–Bulkley fluid model are given. In Section 3, the non-dimensionalisation procedure and the steady flow solution are given. Section 4 deals with the results

analyzing the effect of catheterization on velocity, flow rate, wall shear stress and impedance for different values of the parameters for the Herschel–Bulkley fluid and the results for power law fluid, Newtonian fluid and Bingham fluid are obtained as particular cases.

## 2. Formulation

Consider the flow of blood in an artery in which a catheter is introduced coaxially, where the artery is modeled as a rigid circular tube of radius $\overline{R}$. The catheter radius is taken to be $k\overline{R}$ $(k < 1)$ and the blood is modeled as a Herschel–Bulkley fluid. The flow is assumed to be axially symmetric, laminar, steady and fully developed. It has been observed from the angiographic data on coronary artery that the diameter of the vessel at the upstream and downstream are about 100 μm and 20 μm, respectively [19]. We use the cylindrical polar coordinates $(\bar{r}, \bar{\phi}, \bar{z})$, where $\bar{r}$ and $\bar{z}$ denote the radial and axial coordinates and $\bar{\phi}$ is the azimuthal angle. Fig. 1 shows the flow geometry.

It can be shown that the radial velocity is negligibly small in magnitude and may be neglected for low Reynolds number flow and the pressure gradient is function of $\bar{z}$ alone. The momentum equation in this case simplifies to

$$\frac{\mathrm{d}\bar{p}}{\mathrm{d}\bar{z}} = -\frac{1}{\bar{r}}\frac{\mathrm{d}}{\mathrm{d}\bar{r}}(\bar{r}\bar{\tau}), \quad k\overline{R} \leqslant \bar{r} \leqslant \overline{R}, \tag{1}$$

where $\bar{p}$ denotes the pressure and $\bar{\tau}$ denotes the shear stress. The general form of the constitutive equation for Herschel–Bulkley fluid is taken to be

$$\bar{\eta}\left|\frac{\partial\bar{u}}{\partial\bar{r}}\right| = \left(|\bar{\tau}| - \bar{\tau}_{\mathrm{y}}\right)^{n}, \quad \text{for } |\bar{\tau}| \geqslant \bar{\tau}_{\mathrm{y}}, \tag{2a}$$

$$\frac{\partial\bar{u}}{\partial\bar{r}} = 0, \quad \text{for } |\bar{\tau}| \leqslant \bar{\tau}_{\mathrm{y}}, \tag{2b}$$

where $\bar{\tau}_{\mathrm{y}}$ is the yield stress, $\bar{u}$ is the axial velocity, $n$ is the power index and $\bar{\eta}$ is the coefficient of viscosity for Herschel–Bulkley fluid with dimension $(\mathrm{M\,L^{-1}\,T^{-2}})^{n}\,\mathrm{T}$. The graph explaining the relationship between the shear stress and shear rate is shown in Fig. 2.

The equivalent form of these relations when shear stress and strain rate have opposite signs when $|\bar{\tau}| \geqslant \bar{\tau}_{\mathrm{y}}$ can be written as

$$\bar{\eta}\frac{\partial\bar{u}}{\partial\bar{r}} = \left(|\bar{\tau}| - \bar{\tau}_{\mathrm{y}}\right)^{n}, \quad \text{for } \frac{\partial\bar{u}}{\partial\bar{r}} > 0 \text{ and } \bar{\tau} < 0, \tag{3a}$$

$$= -\left(\bar{\tau} - \bar{\tau}_{\mathrm{y}}\right)^{n}, \quad \text{for } \frac{\partial\bar{u}}{\partial\bar{r}} < 0 \text{ and } \bar{\tau} > 0. \tag{3b}$$

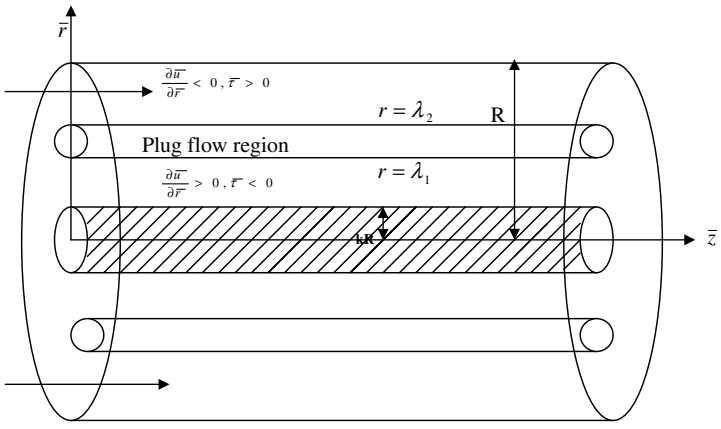


Fig. 1. Geometry of catheterized artery.

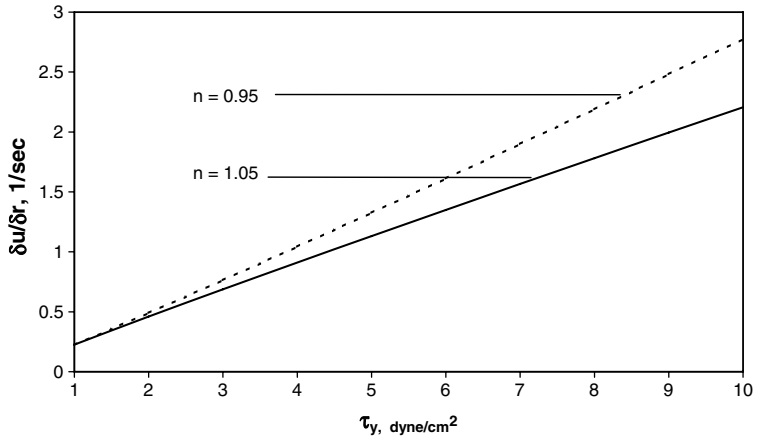


Fig. 2. Variation of shear rate with shear stress for different values of $n$ with $\bar{\tau}_y = 0.1$ dyne/cm$^2$ and $\eta = 4(cP)^n/s^{n-1}$.

For $\frac{\bar{\tau}_y}{|\bar{\tau}|} \ll 1$, the above constitutive equation by neglecting higher powers of $\frac{\bar{\tau}_y}{|\bar{\tau}|}$ can be written as

$$\bar{\eta}\frac{\partial \bar{u}}{\partial \bar{r}} = |\bar{\tau}|^n\left(1 - \frac{n\bar{\tau}_y}{|\bar{\tau}|}\right), \quad \text{if } |\bar{\tau}| \geqslant \bar{\tau}_y \text{ and } \frac{d\bar{u}}{d\bar{r}} > 0, \tag{4a}$$

$$= -|\bar{\tau}|^n\left(1 - \frac{n\bar{\tau}_y}{|\bar{\tau}|}\right), \quad \text{if } |\bar{\tau}| \geqslant \bar{\tau}_y \text{ and } \frac{d\bar{u}}{d\bar{r}} < 0, \tag{4b}$$

$$= 0, \quad \text{if } |\bar{\tau}| < \bar{\tau}_y. \tag{4c}$$

Eqs. (1) and (4) can be solved subject to the no slip boundary conditions on the walls of the catheter and the artery given by

$$\bar{u}(\bar{r} = k\overline{R}) = 0, \tag{5a}$$

$$\bar{u}(\bar{r} = \overline{R}) = 0. \tag{5b}$$

## 3. Method of solution

Let $\bar{p}_0$ be the absolute magnitude of the typical pressure gradient. Let

$$\bar{\mu} = \bar{\eta}\left(\frac{2}{\bar{p}_0\overline{R}}\right)^{n-1}. \tag{6}$$

We introduce the following non-dimensional variables:

$$u = \frac{\bar{u}}{\frac{\bar{p}_0\overline{R}^2}{2\bar{\mu}}}, \quad \tau = \frac{\bar{\tau}}{\frac{\bar{p}_0\overline{R}}{2}}, \quad r = \frac{\bar{r}}{\overline{R}}, \quad z = \frac{\bar{z}}{\overline{R}}. \tag{7}$$

In this case the pressure gradient can be written as

$$\frac{d\bar{p}}{d\bar{z}} = -\bar{p}_0 p_s, \tag{8}$$

where $p_s$ is the non-dimensional steady state pressure gradient. The momentum equation (1) in non-dimensional form is given by

$$2p_s = \frac{1}{r}\frac{d}{dr}(r\tau), \quad k \leqslant r \leqslant 1 \tag{9}$$

and the constitutive equation (4) in the non-dimensional form is

$$\frac{\partial u}{\partial r} = |\tau|^n\left(1-\frac{n\theta}{|\tau|}\right), \quad \text{for } |\tau| \geqslant \theta \text{ and } \frac{\partial u}{\partial r} > 0, \tag{10a}$$

$$= -|\tau|^n\left(1-\frac{n\theta}{|\tau|}\right), \quad \text{for } |\tau| \geqslant \theta \text{ and } \frac{\partial u}{\partial r} < 0, \tag{10b}$$

$$= 0, \quad \text{for } |\tau| < \theta, \tag{10c}$$

where

$$\theta = \frac{2\bar{\tau}_y}{\bar{p}_0\bar{R}} \tag{11}$$

is the non-dimensional yield stress. The boundary conditions (5) reduce to

$$u(r=k) = 0, \tag{12a}$$

$$u(r=1) = 0. \tag{12b}$$

Integration of Eq. (9) yields

$$\tau = p_s r + \frac{C}{r}, \tag{13}$$

where $C$ is the constant of integration. From Eq. (10), it is clear that the flow for $k \leqslant r \leqslant 1$ is a three region one, in which the central core region has a flat velocity profile and hence forms the plug flow region. In this plug flow region, where the shear stress does not exceed the yield stress, the flow is not sheared in the sense that the fluid streamlines are not moving at different velocities. For mathematical representation, let this plug flow region be defined by $\lambda_1 \leqslant r \leqslant \lambda_2$, where $k \leqslant \lambda_1, \lambda_2 \leqslant 1$. Here $\lambda_1$ and $\lambda_2$ are unknown constants to be determined. The three regions are depicted in Fig. 1. From the continuity of the shear stress along the boundary of the plug flow region, we have

$$-\tau|_{r=\lambda_1} = \theta = \tau|_{r=\lambda_2}. \tag{14}$$

Using the above conditions in Eq. (13), we get

$$C = -p_s\lambda^2, \tag{15}$$

where

$$\lambda^2 = \lambda_1\lambda_2. \tag{16}$$

Substitution of Eq. (15) in Eq. (13) yields the shear stress as

$$\tau = \frac{p_s}{r}\left(r^2-\lambda^2\right). \tag{17}$$

Using Eq. (17) and condition (14), we have

$$\lambda_2 - \lambda_1 = \frac{\theta}{p_s} = \beta_s \text{ (say)}, \tag{18}$$

where $\beta_s$ is the width of the plug core region. The expressions for the velocity in three regions can be obtained from Eqs. (17) and (10) and the boundary conditions (12) (see Appendix A) and are given by

$$u^+(r) = p_s^n\left[\int_k^r\left(\frac{\lambda^2-r^2}{r}\right)^n \mathrm{d}r - n\beta_s\int_k^r\left(\frac{\lambda^2-r^2}{r}\right)^{n-1}\mathrm{d}r\right], \quad \text{when } k \leqslant r \leqslant \lambda_1, \tag{19}$$

$$u_p = \text{constant} \quad \text{when } \lambda_1 \leqslant r \leqslant \lambda_2, \tag{20}$$

$$u^{++}(r) = p_s^n\left[\int_r^1\left(\frac{r^2-\lambda^2}{r}\right)^n \mathrm{d}r - n\beta_s\int_r^1\left(\frac{r^2-\lambda^2}{r}\right)^{n-1}\mathrm{d}r\right], \quad \text{when } \lambda_2 \leqslant r \leqslant 1, \tag{21}$$

where $u_p$ denotes the plug flow velocity. When there is no yield stress ($\theta = 0$), we have $\beta_s = 0$. In this case, Eqs. (19) and (21) give the velocity field in a catheterized tube for power law fluid. This agrees with the result quoted by Kapur [20]. Requirement of the continuity of the velocity distribution throughout the flow field leads to the condition

$$u^+(r = \lambda_1) = u_p = u^{++}(r = \lambda_2). \tag{22}$$

This gives

$$\int_k^{\lambda_1} \left(\frac{\lambda^2 - r^2}{r}\right)^n dr - \int_{\lambda_2}^1 \left(\frac{r^2 - \lambda^2}{r}\right)^n dr - n\beta_s \left[\int_k^{\lambda_1} \left(\frac{\lambda^2 - r^2}{r}\right)^{n-1} dr - \int_{\lambda_2}^1 \left(\frac{r^2 - \lambda^2}{r}\right)^{n-1} dr\right] = 0. \tag{23}$$

Using $\lambda^2 = \lambda_1\lambda_2$ and Eq. (18), the above equation reduces to the integral equation in $\lambda_1$ given by

$$\int_k^{\lambda_1} \left(\frac{\lambda_1(\lambda_1 + \beta_s) - r^2}{r}\right)^n dr - \int_{\lambda_1+\beta_s}^1 \left(\frac{r^2 - \lambda_1(\lambda_1 + \beta_s)}{r}\right)^n dr - n\beta_s \left[\int_k^{\lambda_1} \left(\frac{\lambda_1(\lambda_1 + \beta_s) - r^2}{r}\right)^{n-1} dr - \int_{\lambda_1+\beta_s}^1 \left(\frac{r^2 - \lambda_1(\lambda_1 + \beta_s)}{r}\right)^{n-1} dr\right] = 0. \tag{24}$$

The above equation is solved numerically for $\lambda_1$ using Regula–Falsi method, the integrals in Eq. (24) being evaluated using Trapezoidal rule. Once $\lambda_1$ is known, $\lambda_2$ is determined using Eq. (18). The expressions for velocity can be obtained from Eqs. (19)–(21) and using Eq. (16). The steady flow rate $Q_s$ is given by

$$\begin{aligned} Q_s &= 8\int_k^1 ru\,dr \\ &= 4p_s^n \left[-\int_k^{\lambda_1} \left(\frac{\lambda^2 - r^2}{r}\right)^n r^2\,dr + \int_{\lambda_2}^1 \left(\frac{r^2 - \lambda^2}{r}\right)^n r^2\,dr \right. \\ &\quad \left. + n\beta_s \left\{\int_k^{\lambda_1} \left(\frac{\lambda^2 - r^2}{r}\right)^{n-1} r^2\,dr - \int_{\lambda_2}^1 \left(\frac{r^2 - \lambda^2}{r}\right)^{n-1} r^2\,dr\right\}\right]. \end{aligned} \tag{25}$$

The detail of Eq. (25) is given in Appendix B. The wall shear stress in the artery is obtained from Eq. (17) with $r = 1$ and is given by

$$\tau_w = p_s(1 - \lambda^2). \tag{26}$$

For fixed values of $p_s$, the wall shear stress depends on $\lambda$ which in turn depends on $k$ and $\theta$. The frictional resistance per unit length of the artery is given by

$$\Lambda = \frac{p_s}{Q_s}. \tag{27}$$

## 4. Results and discussions

The objective of the present investigation is to understand the fluid mechanics of blood flow in a catheterized artery and to bring out the salient features of the changes in flow pattern and to estimates the increase in flow resistance in a small artery due to the presence of a catheter by modeling blood as a Herschel–Bulkley fluid and the flow is assumed to be steady. The present study also analyses the effects of catheterization and non-Newtonian nature of the fluid on yield plane locations, velocity, flow rate, wall shear stress and resistance to flow. The main advantage of this model is that it incorporates the power law fluid model and Newtonian fluid model as particular cases, so that modeling of blood flow through larger arteries by fluids without yield stress can also be obtained from present analysis. The insertion of a catheter in an artery will increase the frictional resistance to flow through the artery and will modify the pressure distribution.

The yield stress for normal human blood is between 0.01 dyne/s$^2$ and 0.06 dyne/s$^2$, but it is much higher (almost five times) in diseased state for example for a patient with myocardial infarction [21]. Since the value

Table 1
Variation of velocity with radial distance with $p_s = 1$, $\theta = 0.1$ and $k = 0.5$ when $n = 0.75$ and $n = 0.95$

| $r$ | $n = 0.75$ | $n = 0.95$ | Difference |
|---|---|---|---|
| 0.5 | 0 | 0 | 0 |
| 0.52 | 0.01103 | 0.00923 | 0.0018 |
| 0.54 | 0.02094 | 0.01728 | 0.00369 |
| 0.56 | 0.02976 | 0.02419 | 0.00557 |
| 0.58 | 0.03749 | 0.03001 | 0.00748 |
| 0.6 | 0.04413 | 0.03477 | 0.00936 |
| 0.62 | 0.04968 | 0.03851 | 0.01117 |
| 0.64 | 0.0541 | 0.04126 | 0.01284 |
| 0.66 | 0.05736 | 0.04302 | 0.01434 |
| 0.68 | 0.05938 | 0.04382 | 0.01556 |
| 0.7 | 0.05976 | 0.04387 | 0.01589 |
| 0.72 | 0.05976 | 0.04387 | 0.01589 |
| 0.74 | 0.05976 | 0.04387 | 0.01589 |
| 0.76 | 0.05976 | 0.04387 | 0.01589 |
| 0.78 | 0.05976 | 0.04387 | 0.01589 |
| 0.8 | 0.05892 | 0.04353 | 0.01539 |
| 0.82 | 0.05672 | 0.04238 | 0.01434 |
| 0.84 | 0.05353 | 0.04047 | 0.01306 |
| 0.86 | 0.04944 | 0.0378 | 0.01164 |
| 0.88 | 0.04452 | 0.03442 | 0.0101 |
| 0.9 | 0.03882 | 0.03034 | 0.00848 |
| 0.92 | 0.03239 | 0.02557 | 0.00682 |
| 0.94 | 0.02526 | 0.02014 | 0.00512 |
| 0.96 | 0.01747 | 0.01406 | 0.00341 |
| 0.98 | 0.00904 | 0.00734 | 0.0017 |
| 1 | 0 | 0 | 0 |

of $\bar{\tau}_y$ is 0.04 dyne/s$^2$ for blood at haematocrit of 40 [22], the non-Newtonian effects are more pronounced as $\theta$ value increases and Eq. (11) suggests that it should be true for flow in narrow blood vessels where the pressure gradient is also very small. In large vessels in which pressure gradient is large, $\theta$ is negligible and blood behaves more like a Newtonian fluid. As suggested by Dash et al. [10], we have taken the value of $\theta$ to range from 0 to 0.3, as this range is more suitable for all vessels through which a catheter is inserted. Similarly, the values of catheter radius ratio $k$ have been taken to range from 0.1 to 0.7 to accommodate all types of catheter and also to pronounce the difference in the flow quantities due to the increase of catheter radius ratio $k$.

It is generally observed that the typical value of the power index $n$ for blood flow are taken to lie between 0.9 and 1.1 and we have taken a typical value of $n$ to be 0.95 for $n < 1$ and 1.05 for $n > 1$. The data for variation of velocity with radial distance '$r$' for $n = 0.75$ and $n = 0.95$ and the difference between these values are given in Table 1. The data for variation of flow rate with steady pressure gradient $p_s$ for $n = 0.75$ and $n = 0.95$ and the difference between these values are given in Table 2. We noticed that there is not much of difference in the flow quantities given in Tables 1 and 2 when $n = 0.75$ and $n = 0.95$. A similar pattern is observed when $n = 1.05$ and $n = 1.25$. So we are content with giving the typical values of power index $n$ as 0.95 when $n < 1$ and 1.05 when $n > 1$.

Steady flow experiments in vitro on the flow of blood through small tubes indicate that blood possess finite yield stress, shear-dependent viscosity and relatively a cell-free layer (plasma layer) near a tube wall. This later effect is related to a phase separation of red cell and plasma, due primarily to a volume exclusion at the boundary and could be considered a departure from a single phase continuum, while a yield stress and shear-dependent viscosity are interpreted as manifestations of non-Newtonian but still continuum behaviour [23]. The effect of finite yield stress is that the fluid exhibits solid like behaviour or plug flow (where all velocity gradients are negligible) in regions where the shear stress is less than the yield stress. The location of a point where the yield stress is equal to the actual stress value is called a yield point and the locus of such points is called yield surface or yield plane. In the case of a tube flow we have only one yield plane whereas for annular flow there are two yield planes $r = \lambda_1$ and $r = \lambda_2$ and these two yield planes determine the plug flow region in the annular

Table 2
Variation of flow rate with steady pressure gradient with $\theta = 0.1$ and $k = 0.5$ when $n = 0.75$ and $n = 0.95$

| $p_s$ | $n = 0.75$ | $n = 0.95$ | Difference |
|---|---|---|---|
| 1 | 0.125191 | 0.095145 | 0.030046 |
| 2 | 0.242249 | 0.21963 | 0.022619 |
| 3 | 0.342804 | 0.340664 | 0.00214 |
| 4 | 0.43436 | 0.459485 | 0.025125 |
| 5 | 0.519873 | 0.57671 | 0.056837 |
| 6 | 0.600928 | 0.692727 | 0.091799 |
| 7 | 0.67851 | 0.807708 | 0.129198 |
| 8 | 0.753229 | 0.921823 | 0.168594 |
| 9 | 0.825557 | 1.03522 | 0.209663 |
| 10 | 0.895837 | 1.147941 | 0.252104 |

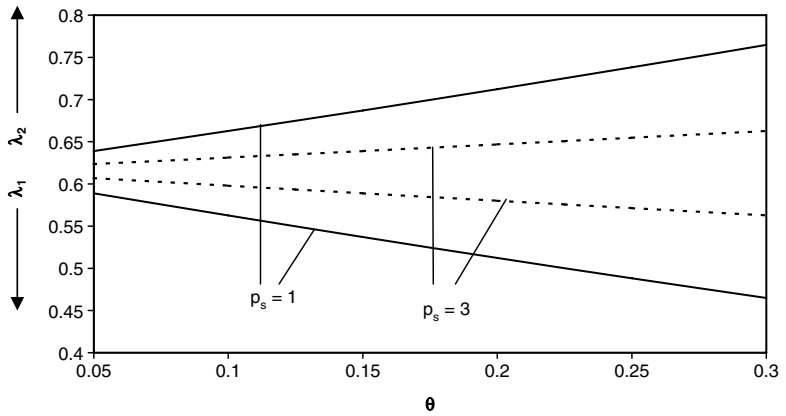


Fig. 3. Variation of yield plane location with yield stress $\theta$ for different values of pressure gradient $p_s$ when $n = 0.95$ and $k = 0.3$.

region. The values of $\lambda_1$ and $\lambda_2$ are determined by solving Eqs. (24) and (18). In steady flow the yield plane locations $\lambda_1$ and $\lambda_2$ do not change during the course of motion. The locations of the yield planes $\lambda_1$ and $\lambda_2$ with yield stress $\theta$ for different values of pressure gradient $p_s$ when $n = 0.95$ and $k = 0.3$ are shown in Fig. 3. The value of $\lambda_1$ increases and the width of the plug core region decreases with increasing pressure gradient for a given value of $n$, $k$ and $\theta$. The width of the plug core increases with increasing value of the yield stress $\theta$ for a given value of a pressure gradient as can be seen from Eq. (18), although the value of $\lambda_1$ decreases with increasing $\theta$.

The effect of non-Newtonian nature of the fluid on the velocity distribution for a given catheter radius ratio for various values of yield stress $\theta$ when $k = 0.5$ and $p_s = 1$ for $n = 0.95$ and $n = 1.05$ is depicted in Fig. 4a and b, respectively. It is observed that the velocity distribution for Newtonian fluid ($\theta = 0$ and $n = 1$), the maximum velocity is slightly skewed towards the inner wall of the annulus which is a well known result for Newtonian fluid. As $\theta$ increases the width of the plug core region increases and the velocity decreases considerably and for $\theta = 0.3$ the plug core region is almost the entire annulus region, the velocity in the plug core region being almost zero. The plug flow region is skewed slightly towards the inner wall of the annulus. Also as $n$ increases the velocity decreases for a given value of $k$ and $\theta$ when $p_s = 1$. From Fig. 4a and b, it is obvious that the power law fluid velocities are much higher compare to fluids with yield stress and the velocity for power law fluid with $n = 0.95$ is greater than that of Newtonian fluid. For easy comparison the velocity profiles for different fluid are given in Fig. 5. It is noted that for each value of the yield stress the velocity distribution for Casson fluid obtained by Dash et al. [10] are much lower than those of Herschel–Bulkley fluids.

The variation of plug flow velocity with catheter ratio $k$ with $n = 0.95$ for different values of yield stress $\theta$ is shown in Fig. 6. The plug flow velocity decreases rapidly as $k$ increases from 0 to 0.15 for each value of $\theta$ and the velocity decreases gradually as $k$ increases from 0.15 to 0.7. For $\theta = 0.25$, the plug flow velocity becomes

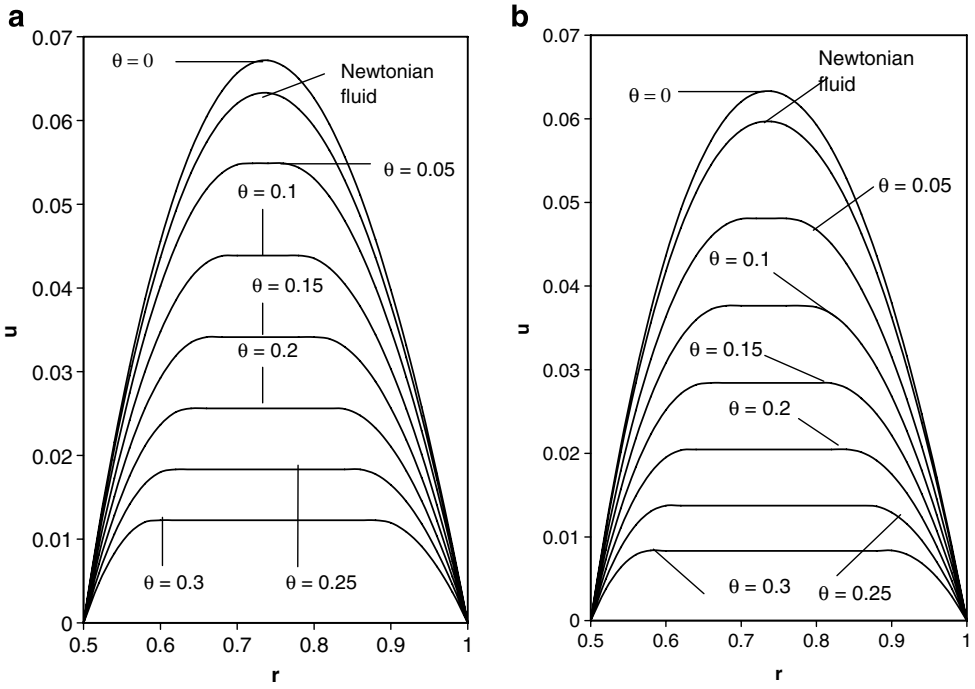


Fig. 4. Velocity distribution for different values of yield stress $\theta$ with $k = 0.5$ and $p_s = 1$. (a) $n = 0.95$, (b) $n = 1.05$.

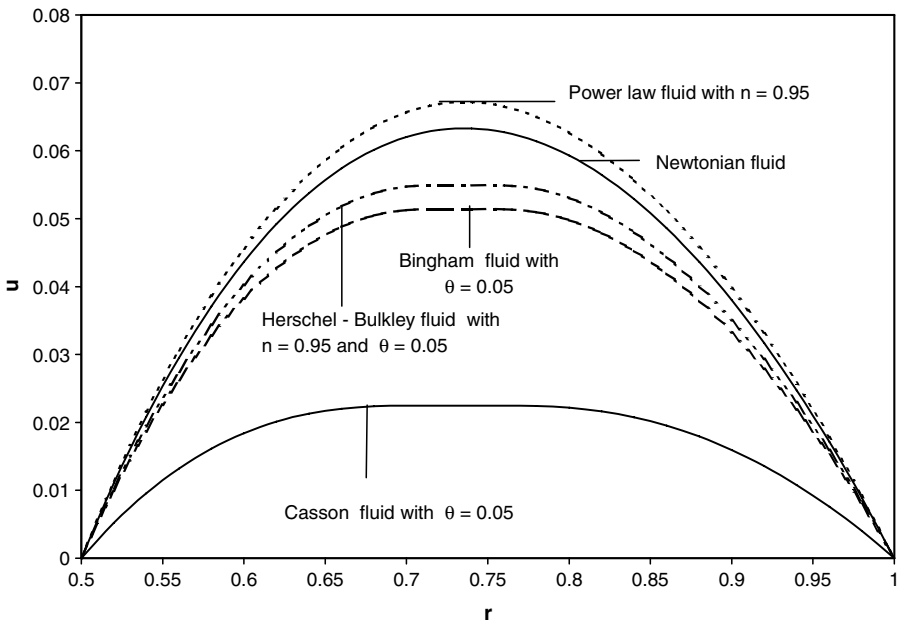


Fig. 5. Velocity distribution for different fluids with $p_s = 1$.

zero and when $k$ is nearly 0.7, whereas for Casson fluid the plug core velocity is zero approximately at $k = 0.55$ [10]. In these cases the whole flow region is almost plugged for respective values of $k$ although the actual width of the plug flow region is 0.25.

The flow rate $Q_s$ is given by Eq. (25). Fig. 7 shows the variation of flow rate with yield stress for different values of catheter radius ratio $k$ under unit pressure gradient. When $n = 0.95$ the flow rate decreases almost

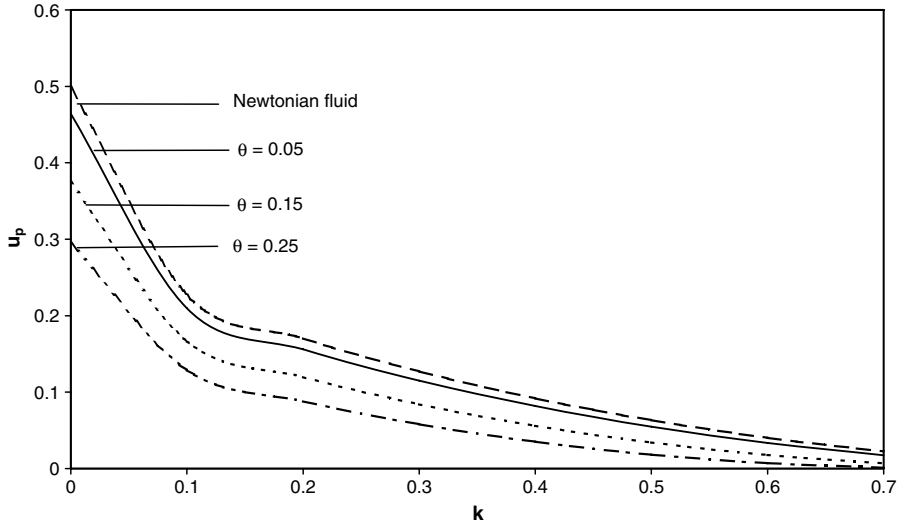


Fig. 6. Variation of plug flow velocity with catheter radius ratio $k$ for different values of yield stress $\theta$ with $p_s = 1$ and $n = 0.95$.

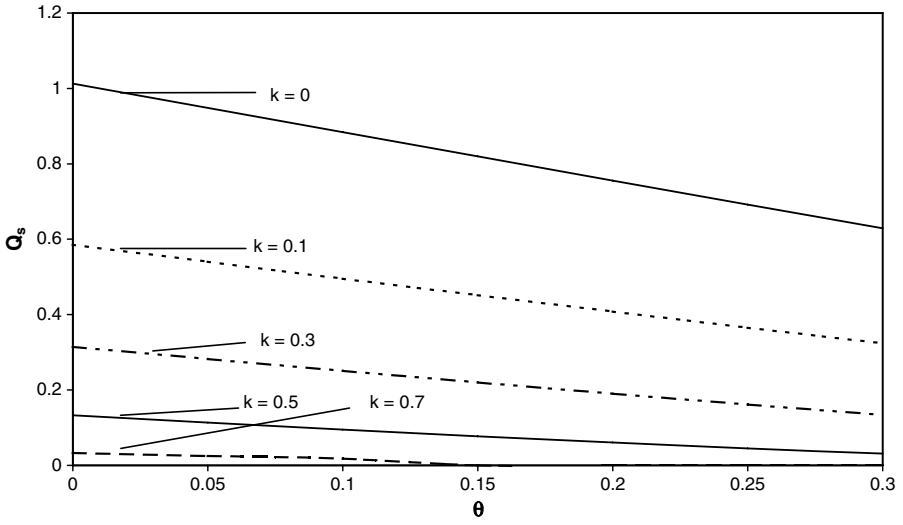


Fig. 7. Variation of flow rate with yield stress for different values of catheter radius ratio $k$ with $p_s = 1$ and $n = 0.95$.

linearly whereas for Casson fluid the variation is highly non-linear and steeply decreases as the yield stress increases from 0 to 0.1 for a given catheter radius. This is mainly due to the increase in the width of the plug core region. For a fixed yield stress, the flow rate decreases more rapidly as the catheter radius ratio increases which is due to the reduction in the annular flow region. The flow is almost stopped when $k = 0.7$ at $\theta = 0.13$. Thus Figs. 6 and 7 describe the simultaneous effects of non-Newtonian nature of the fluid and catheterization for a given pressure gradient.

Fig. 8 shows the variation of steady flow rate with pressure gradient for different values of $\theta$ with $k = 0.4$ when $n = 0.95$. It is seen that the variation is not much with variation in $\theta$.

A basic aim of problems related to physiological fluid dynamics is to predict wall shear stress in arteries which significantly influences the rate of mass transport across the artery walls and the possible development of atherogenesis. In steady flow the wall shear stress is calculated from Eq. (26). It is obvious that for a fixed $p_s$, the wall shear stress depends on $\lambda$ and in turn $\lambda$ depends on $k$ and $\theta$.

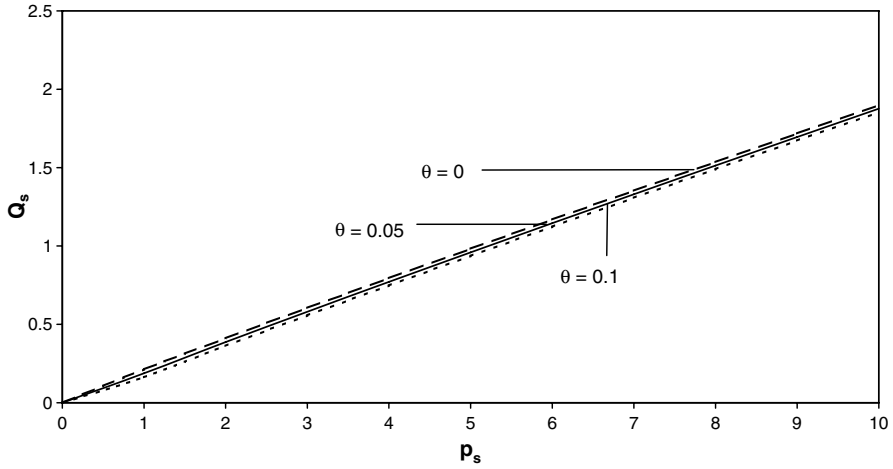


Fig. 8. Variation of flow rate with pressure gradient $p_s$ for different values of yield stress $\theta$ with catheter radius ratio $k = 0.4$ and $n = 0.95$.

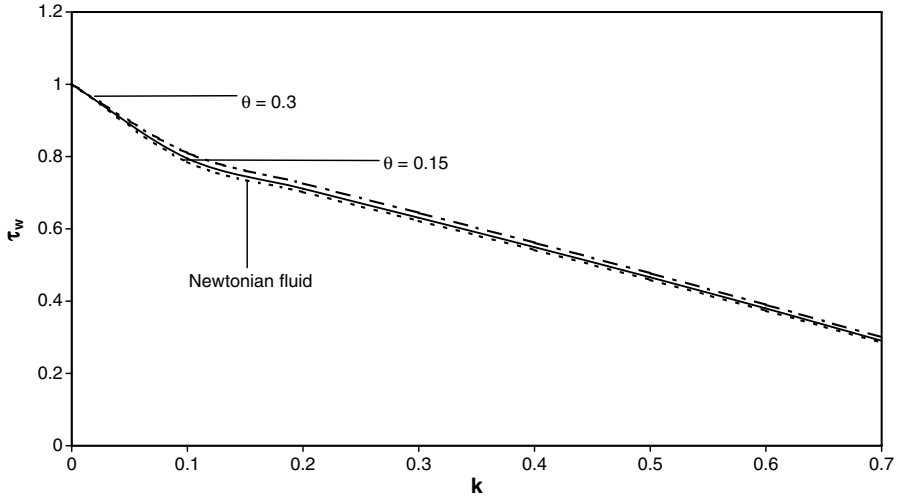


Fig. 9. Variation of wall shear stress with catheter radius ratio $k$ for different values of yield stress $\theta$ with $p_s = 1$ and $n = 0.95$.

The variation of wall shear stress with catheter radius ratio $k$ for different values of yield stress $\theta$ when $n = 0.95$ and $p_s = 1$ is shown in Fig. 9. This figure again depicts the simultaneous effects of the non-Newtonian nature of the fluid and catheterization. It is observed that for a given pressure gradient the walls shear stress decreases as the catheter radius ratio $k$ increases and in particular decreases very rapidly from $k = 0$ to $k = 0.1$. For a fixed catheter radius ratio $k$, the wall shear stress increases marginally as the yield stress $\theta$ increases.

The frictional resistance ($\Lambda$) per unit length of the artery is calculated using Eq. (27). It is clear that under a given pressure gradient a greater resistance implies less flow of fluid. Thus the resistance gives the measure of the volume of the fluid transported by the artery. Fig. 10a and b show the variation of frictional resistance with catheter radius ratio $k$ for different values of the yield stress $\theta$ and for unit pressure gradient when $n = 0.95$ and $n = 1.25$, respectively. The frictional resistance increases with increasing $k$ and it also increases with increasing $\theta$. Therefore the frictional resistance is more for Herschel–Bulkley fluid compared to power law fluid for a given $n$. When $p_s = 1$, the frictional resistance is more for Herschel–Bulkley fluid with $n = 1.05$ compared to Herschel–Bulkley fluid with $n = 0.95$. The difference is not much for small values of $k$ (0.1–0.3) and for small values of $\theta$ (0.1–0.2). When $\theta = 0.3$ and $k = 0.6$, the frictional resistance for Herschel–Bulkley fluid with $n = 1.05$ is almost double to Herschel–Bulkley fluid with $n = 0.95$.

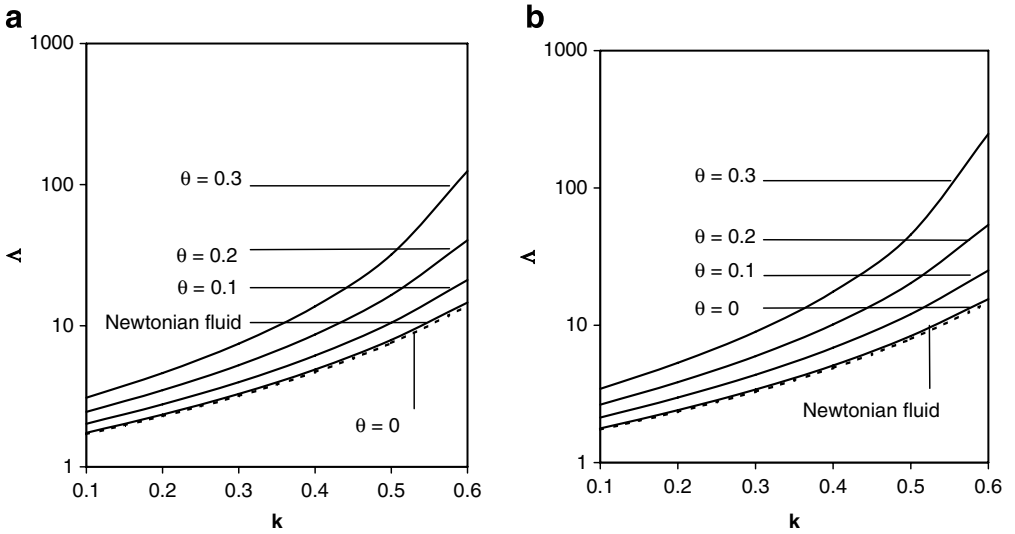


Fig. 10. Variation of frictional resistance with catheter radius ratio $k$ for different values of yield stress $\theta$ with $p_s = 1$. (a) $n = 0.95$, (b) $n = 1.05$.

Table 3
Frictional resistance increase for Casson fluid with $p_s = 1$

| $k$ | $\theta$ | | | | | | |
|---|---|---|---|---|---|---|---|
| | 0.0 | 0.05 | 0.1 | 0.15 | 0.2 | 0.25 | 0.3 |
| 0.1 | 1.7414 | 3.3036 | 4.6153 | 6.2077 | 8.2519 | 10.9642 | 14.66815 |
| 0.2 | 2.3486 | 4.705 | 6.8107 | 9.4972 | 13.13 | 18.2309 | 25.65271 |
| 0.3 | 3.2885 | 7.0112 | 10.591 | 15.447 | 22.462 | 33.0806 | 49.96608 |
| 0.4 | 4.8938 | 11.271 | 17.999 | 27.906 | 43.592 | 70.0915 | 118.4054 |
| 0.5 | 7.9375 | 20.239 | 34.951 | 59.327 | 103.77 | 193.714 | 403.6217 |
| 0.6 | 14.586 | 42.965 | 83.797 | 165.73 | 357.98 | 918.887 | 3328.362 |

We reproduce the table given by Dash et al. [10] for frictional resistance increase factor for Casson fluid in Table 3. But we realized that what they have tabulated is actual frictional resistance and not the increase in frictional resistance. If we define the frictional resistance increase factor as the ratio of frictional resistance for Casson fluid in the catheterized artery to the frictional resistance of Newtonian fluid in the uncatheterized artery, the values in Table 3 will represent this frictional resistance increase.

In this case the increase denotes the simultaneous effects of non-Newtonian nature of the fluid and the catheterization. These values for Herschel–Bulkley fluid for $n = 0.95$ and $n = 1.05$ are tabulated in Tables 4 and 5. It is noticed that depending on the catheter radius ratio $k$ which varies from 0.3 to 0.6, the flow resistance increases by a factor 3.29–14.58 for Newtonian fluid. In small blood vessels, where non-Newtonian nature

Table 4
Frictional resistance increase for Herschel–Bulkley fluid with effects on non-Newtonian nature when $n = 0.95$ and $p_s = 1$

| $k$ | $\theta$ | | | | | | | |
|---|---|---|---|---|---|---|---|---|
| | Newtonian fluid | Power law | 0.05 | 0.1 | 0.15 | 0.2 | 0.25 | 0.3 |
| 0.1 | 1.7413 | 1.7091 | 1.8512 | 2.018 | 2.2155 | 2.45161 | 2.7374 | 3.08813 |
| 0.2 | 2.3485 | 2.2880 | 2.5082 | 2.7731 | 3.0955 | 3.49281 | 3.99067 | 4.62664 |
| 0.3 | 3.2883 | 3.1799 | 3.5378 | 3.9815 | 4.5401 | 5.25675 | 6.19752 | 7.46785 |
| 0.4 | 4.8935 | 4.6938 | 5.3251 | 6.1400 | 7.215 | 8.67354 | 10.72417 | 13.7421 |
| 0.5 | 7.9372 | 7.5417 | 8.7960 | 10.5100 | 12.935 | 16.5246 | 22.17703 | 31.8887 |
| 0.6 | 14.585 | 13.702 | 16.675 | 21.1200 | 28.175 | 40.4009 | 64.61481 | 124.63 |

Table 5
Frictional resistance increase for Herschel–Bulkley fluid with effects on non-Newtonian nature when $n = 1.05$ and $p_s = 1$

| $k$ | $\theta$ | | | | | | | |
|---|---|---|---|---|---|---|---|---|
| | Newtonian fluid | Power law | 0.05 | 0.1 | 0.15 | 0.2 | 0.25 | 0.3 |
| 0.1 | 1.7413 | 1.7736 | 1.9349 | 2.1275 | 2.3598 | 2.64395 | 2.99668 | 3.44283 |
| 0.2 | 2.3485 | 2.41 | 2.6642 | 2.9759 | 3.3637 | 3.85461 | 4.48958 | 5.33164 |
| 0.3 | 3.2883 | 3.3995 | 3.8196 | 4.3522 | 5.0411 | 5.95416 | 7.20205 | 8.97418 |
| 0.4 | 4.8935 | 5.1005 | 5.8552 | 6.8562 | 8.2219 | 10.1553 | 13.02632 | 17.5723 |
| 0.5 | 7.9372 | 8.3507 | 9.883 | 12.05 | 15.254 | 20.2915 | 28.91379 | 45.6856 |
| 0.6 | 14.585 | 15.52 | 19.252 | 25.091 | 34.993 | 53.9087 | 97.86211 | 247.763 |

of blood must be taken into account, the value of yield stress possessed by blood can cause even more increase in flow resistance. For Herschel–Bulkley fluid with $n = 0.95$ and with the same range of catheter radius ratio (i.e. $k$ varies from 0.3 to 0.6), the frictional resistance increases by a factor of 3.98–21.12 when $\theta = 0.1$ and 7.47–124.6 when $\theta = 0.3$ whereas for Herschel–Bulkley fluid with $n = 1.05$, these factors are 4.35–25.09 when $\theta = 0.1$ and 8.97–247.76 when $\theta = 0.3$. Dash et al. [10] have shown for the same range of catheter radius ratio ($k$ ranges from 0.3 to 0.6), the frictional resistance increases by a factor 10.59–83.79 when $\theta = 0.1$ and 49.97–3328.36 when $\theta = 0.3$ for Casson fluid.

If we have to compare only the effect of catheterization alone for a particular fluid then we must define the frictional resistance increase factor as the ratio of frictional resistance for catheterized artery to that in uncatheterized artery for the particular fluid. Therefore to find the increase in frictional resistance due to catheterization alone for Herschel–Bulkley fluid, we define the frictional resistance increase as the ratio of frictional resistance for catheterized artery for given values of $n$ and $\theta$ to the frictional resistance of uncatheterized artery for the same values of $n$ and $\theta$. In this case the frictional resistance increase when $k$ ranges from 0.3 to 0.6 are 3.52–18.67 for $n = 0.95$ and 3.7–21.33 for $n = 1.05$ when $\theta = 0.1$ and 4.7–78.35 for $n = 0.95$ and 5.18–143.1 for $n = 1.05$ when $\theta = 0.3$ for unit pressure gradient. The corresponding increase in frictional resistance for Casson fluid are 4.35–34.4 when $\theta = 0.1$ and 7.38–491.38 when $\theta = 0.3$ and for Newtonian fluid it is 3.29–14.59. The detailed values are given in Tables 6 and 7. Therefore for relatively large values of $k$ and $\theta$, the frictional

Table 6
Frictional resistance increase for Herschel–Bulkley fluid with effects on catheterization when $n = 0.95$ and $p_s = 1$

| $k$ | $\theta$ | | | | | | | |
|---|---|---|---|---|---|---|---|---|
| | Newtonian fluid | Power law | 0.05 | 0.1 | 0.15 | 0.2 | 0.25 | 0.3 |
| 0.1 | 1.7413 | 0.7182 | 1.7556 | 1.7838 | 1.8159 | 1.85234 | 1.89379 | 1.94128 |
| 0.2 | 2.3485 | 2.3172 | 3.3787 | 2.4513 | 2.5372 | 2.63903 | 2.76083 | 2.90843 |
| 0.3 | 3.2883 | 3.2204 | 3.355 | 3.5195 | 3.7213 | 3.97179 | 4.28758 | 4.69449 |
| 0.4 | 4.8935 | 4.7536 | 5.05 | 5.4274 | 5.9138 | 6.55336 | 7.41921 | 8.63862 |
| 0.5 | 7.9372 | 7.6379 | 8.3416 | 9.2905 | 10.602 | 12.4861 | 14.65072 | 20.0461 |
| 0.6 | 14.585 | 13.877 | 15.814 | 18.669 | 23.093 | 30.5253 | 44.7019 | 78.3455 |

Table 7
Frictional resistance increase for Herschel–Bulkley fluid with effects on catheterization when $n = 1.05$ and $p_s = 1$

| $k$ | $\theta$ | | | | | | | |
|---|---|---|---|---|---|---|---|---|
| | Newtonian fluid | Power law | 0.05 | 0.1 | 0.15 | 0.2 | 0.25 | 0.3 |
| 0.1 | 1.7413 | 1.7518 | 1.778 | 1.8085 | 1.8438 | 1.88481 | 1.93243 | 1.98841 |
| 0.2 | 2.3485 | 2.3805 | 2.4481 | 2.5297 | 2.6282 | 2.74786 | 2.89514 | 3.07929 |
| 0.3 | 3.2883 | 3.3579 | 3.5098 | 3.6996 | 3.9155 | 4.23562 | 4.6443 | 5.18304 |
| 0.4 | 4.8935 | 5.038 | 5.3804 | 5.8328 | 6.4241 | 7.23948 | 8.40012 | 10.1489 |
| 0.5 | 7.9372 | 8.2485 | 9.0813 | 10.243 | 11.919 | 14.4653 | 18.64528 | 26.3858 |
| 0.6 | 14.585 | 15.33 | 17.691 | 21.329 | 27.342 | 38.4302 | 63.10712 | 143.096 |

Table 8
Catheter types, sizes and measurements

| Type | Size (diameter) $d_i$ (mm) | Measurement | Source |
|---|---|---|---|
| Angioplasty catheter guide wire | 0.356 | $\Delta P$ Pressure drop | Wilson et al. [2] |
| Coronary angioplasty catheter | 1.4 | $\Delta P$ Pressure $p$ distal to lesion | Wilson et al. [2] |
| Guiding catheter | 2.6 | $\Delta P$ Pressure $p$ at coronary ostium | Wilson et al. [2] |
| Doppler catheter | 1.0 | Velocity $u$ proximal to lesion | Johnson et al. [24] |
| Coronary infusion catheter | 0.66 | $\Delta P$ Pressure drop across lesion | Ganz et al. [25] |

Table 9
Range of flow resistance increase for different types of catheter and for different fluids

| Type | Range of $d_i/d_0$ | Range of flow resistance increase | | | |
|---|---|---|---|---|---|
| | | Newtonian fluid | Herschel–Bulkley fluid | | Casson fluid $\theta = 0.1$ |
| | | | $n = 0.95$; $\theta = 0.1$ | $n = 1.05$; $\theta = 0.1$ | |
| Guide wire | 0.08–0.8 | 1.64–2.21 | 1.68–2.29 | 1.69–2.36 | 1.75–2.57 |
| Infusion | 0.14–0.33 | 1.96–3.68 | 2.02–3.97 | 2.06–4.2 | 2.2–5.03 |
| Angioplasty catheter | 0.3–0.6 | 3.29–14.58 | 3.52–18.67 | 3.7–21.33 | 4.34–34.4 |

resistance increases several hundred times to obstruct the fluid movement considerably for non-Newtonian fluids.

For comparisons of the results with different types of catheters used, we reproduce the table given by Back [1] in Table 8. Table 9 gives the range of flow resistance increase for different catheter types for Newtonian fluid given by Back [1] with results of Herschel–Bulkley and Casson fluid is incorporated and this is the effect of catheterization alone on frictional resistance increase for unit pressure gradient. In Table 9, $d_i$ denotes the diameter of catheter and $d_0$ denotes the diameter of artery.

## 5. Conclusion

In this paper the effect of catheterization on pressure distribution, wall shear stress and the resistance to flow are discussed by modeling blood by Herschel–Bulkley fluid and the blood vessels and the catheter by coaxial rigid tubes. The velocity decreases and the width of the plug core region increases as the yield stress increases. The velocity for Herschel–Bulkley fluid is higher than that of Casson fluid and lower than that of power law fluid for a given $p_s$, $\theta$, $k$ and $n$. The flow rate decreases with increasing yield stress and also with increasing catheter radius ratio $k$, but increases with increasing pressure gradient $p_s$. The wall shear stress decreases as the catheter radius ratio $k$ increases but it increases when the yield stress $\theta$ increases for a given value of $p_s$ and $n$.

The frictional resistance increases with increasing catheter radius ratio $k$ and with increasing yield stress $\theta$ for a given values of $n$ and $p_s$ as expected. The values of frictional resistance for Herschel–Bulkley fluid for a given $p_s$, $\theta$, $k$ and $n$, are lower than those of Casson fluid but higher than that of power law fluid. It is to be noted that frictional resistance increases with increasing catheter radius ratio and is much higher for Herschel–Bulkley fluid with $n = 1.05$ compared to that of Herschel–Bulkley fluid with $n = 0.95$, for unit pressure gradient. The increase in flow resistance due to catheterization alone and also that due to the simultaneous effects of non-Newtonian nature and catheterization are obtained for Herschel–Bulkley fluid and compared with Casson and Newtonian fluids. We hope that this theoretical work will be of use for experimental work by other researchers.

## Acknowledgement

The authors thank Prof. P. Chaturani, Department of Mathematics, Indian Institute of Technology, Bombay, for his valuable suggestions and timely help in the preparation of the paper.

## Appendix 1

Using $|\tau| = -\tau$ in Eq. (10a) and making use of Eq. (17), we get

$$\frac{du^+}{dr} = p_s^n\left[\left(\frac{\lambda^2 - r^2}{r}\right)^n - n\beta_s\left(\frac{\lambda^2 - r^2}{r}\right)^{n-1}\right]. \tag{A.1}$$

Integration of Eq. (A.1) with respect to $r$ from $k$ to $r$ with the help of boundary condition (12a), yields

$$u^+(r) = p_s^n\left[\int_k^r \left(\frac{\lambda^2 - r^2}{r}\right)^n dr - n\beta_s\int_k^r \left(\frac{\lambda^2 - r^2}{r}\right)^{n-1} dr\right]. \tag{A.2}$$

From Eqs. (17) and (10a) with $|\tau| = \tau$, we get

$$\frac{du^{++}}{dr} = -p_s^n\left[\left(\frac{r^2 - \lambda^2}{r}\right)^n - n\beta_s\left(\frac{r^2 - \lambda^2}{r}\right)^{n-1}\right]. \tag{A.3}$$

Integrating Eq. (A.3) with respect to $r$ from $r$ to 1 and using boundary condition (12b), we get

$$u^{++}(r) = p_s^n\left[\int_r^1 \left(\frac{r^2 - \lambda^2}{r}\right)^n dr - n\beta_s\int_r^1 \left(\frac{r^2 - \lambda^2}{r}\right)^{n-1} dr\right]. \tag{A.4}$$

## Appendix 2

The steady flow rate $Q_s$ is given by

$$Q_s = 8\int_k^1 ru\,dr = 8\left[\int_k^{\lambda_1} ru^+\,dr + \int_{\lambda_1}^{\lambda_2} ru_p\,dr + \int_{\lambda_2}^1 ru^{++}\,dr\right] = 8(Q_1 + Q_2 + Q_3). \tag{A.5}$$

Substituting Eq. (19) in $Q_1$, we get

$$Q_1 = p_s^n\left[\int_{r=k}^{\lambda_1}\int_{x=k}^{r}\left(\frac{\lambda^2 - x^2}{x}\right)^n dx\,r\,dr - n\beta_s\int_{r=k}^{\lambda_1}\int_{x=k}^{r}\left(\frac{\lambda^2 - x^2}{x}\right)^{n-1} dx\,r\,dr\right]. \tag{A.6}$$

Change of order of integrals in Eq. (A.6) gives

$$Q_1 = p_s^n\left[\int_k^{\lambda_1}\left(\frac{\lambda_1^2 - x^2}{2}\right)\left(\frac{\lambda^2 - x^2}{x}\right)^n dx - n\beta_s\int_k^{\lambda_1}\left(\frac{\lambda_1^2 - x^2}{2}\right)\left(\frac{\lambda^2 - x^2}{x}\right)^{n-1} dx\right]. \tag{A.7}$$

Using the first part of condition (22) in Eq. (19), the plug flow velocity $u_p$ is obtained as

$$u_p = p_s^n\left[\int_k^{\lambda_1}\left(\frac{\lambda^2 - r^2}{r}\right)^n dr - n\beta_s\int_k^{\lambda_1}\left(\frac{\lambda^2 - r^2}{r}\right)^{n-1} dr\right]. \tag{A.8}$$

This gives value of $Q_2$ as

$$Q_2 = p_s^n\left[\int_k^{\lambda_1}\left(\frac{\lambda_2^2 - \lambda_1^2}{2}\right)\left(\frac{\lambda^2 - x^2}{x}\right)^n dx - n\beta_s\int_k^{\lambda_1}\left(\frac{\lambda_2^2 - \lambda_1^2}{2}\right)\left(\frac{\lambda^2 - x^2}{x}\right)^{n-1} dx\right]. \tag{A.9}$$

Similarly we obtain

$$Q_3 = p_s^n\left[\int_{r=\lambda_2}^{1}\int_{x=r}^{1}\left(\frac{x^2 - \lambda^2}{x}\right)^n dx\,r\,dr - n\beta_s\int_{r=\lambda_2}^{1}\int_{x=r}^{1}\left(\frac{x^2 - \lambda^2}{x}\right)^{n-1} dx\,r\,dr\right]. \tag{A.10}$$

Change of order of integrals in $Q_3$ gives

$$Q_3 = p_s^n \left[ \int_{\lambda_2}^{1} \left( \frac{x^2 - \lambda_2^2}{2} \right) \left( \frac{x^2 - \lambda^2}{x} \right)^n \mathrm{d}x - n\beta_s \int_{\lambda_2}^{1} \left( \frac{x^2 - \lambda_2^2}{2} \right) \left( \frac{x^2 - \lambda^2}{x} \right)^{n-1} \mathrm{d}x \right]. \tag{A.11}$$

The value of $Q_s$ simplifies to

$$\begin{aligned} Q_s = 4p_s^n \Bigg[ & - \int_k^{\lambda_1} \left( \frac{\lambda^2 - r^2}{r} \right)^n r^2 \,\mathrm{d}r + n\beta_s \int_k^{\lambda_1} \left( \frac{\lambda^2 - r^2}{r} \right)^{n-1} r^2 \,\mathrm{d}r + \int_{\lambda_2}^{1} \left( \frac{r^2 - \lambda^2}{r} \right)^n r^2 \,\mathrm{d}r - n\beta_s \int_{\lambda_2}^{1} \left( \frac{r^2 - \lambda^2}{r} \right)^{n-1} r^2 \,\mathrm{d}r \\ & + \lambda_2^2 \left\{ \left[ \int_k^{\lambda_1} \left( \frac{\lambda^2 - r^2}{r} \right)^n \mathrm{d}r - n\beta_s \int_k^{\lambda_1} \left( \frac{\lambda^2 - r^2}{r} \right)^{n-1} \mathrm{d}r \right] - \left[ \int_{\lambda_2}^{1} \left( \frac{r^2 - \lambda^2}{r} \right)^n \mathrm{d}r - n\beta_s \int_{\lambda_2}^{1} \left( \frac{r^2 - \lambda^2}{r} \right)^{n-1} \mathrm{d}r \right] \right\} \Bigg]. \end{aligned} \tag{A.12}$$

The condition (22) gives

$$\int_k^{\lambda_1} \left( \frac{\lambda^2 - r^2}{r} \right)^n \mathrm{d}r - n\beta_s \int_k^{\lambda_1} \left( \frac{\lambda^2 - r^2}{r} \right)^{n-1} \mathrm{d}r = \int_{\lambda_2}^{1} \left( \frac{r^2 - \lambda^2}{r} \right)^n \mathrm{d}r - n\beta_s \int_{\lambda_2}^{1} \left( \frac{r^2 - \lambda^2}{r} \right)^{n-1} \mathrm{d}r. \tag{A.13}$$

Using the above in Eq. (A.12), we get Eq. (25).

## References


[1] L.H. Back, Estimated mean flow resistance increase during coronary artery catheterization, J. Biomech. 27 (2) (1994) 169–175.
[2] R.F. Wilson, M.R. Johnson, M.L. Marcus, P.E.G. Alyward, D.J. Skorton, S. Collings, C.W. White, The effect of coronary angioplasty on coronary flow reserve, Circulation 77 (1988) 873–885.
[3] H.V. Anderson, G.S. Roubin, P.P. Leimgruber, W.R. Cox, J.S. Douglas, S.B. Kings Jr, A.R. Gruentzig, Measurement of transstenotic pressure gradient during percutaneous transluminal angioplasty, Circulation 73 (1986) 1223–1230.
[4] L.H. Back, T.A. Denton, Some arterial wall shear stress estimates in coronary angioplasty, Adv. Bioeng. 22 (1992) 337–340.
[5] L.H. Back, E.Y. Kwack, M.R. Back, Flow rate-pressure drop relation in coronary angioplasty: catheter obstruction effect, J. Biomech. Eng. Trans. ASME 118 (1996) 83–89.
[6] J. Aroesty, J.F. Gross, Pulsatile flow in small vessels – I. Casson theory, Biorheology 9 (1972) 33–42.
[7] P. Chaturani, R. Ponnalagar Samy, Pulsatile flow of a Casson fluid through stenosed arteries with application to blood flow, Biorheology 23 (1986) 499–511.
[8] G.T. Karahalios, Some possible effects of a catheter on the arterial wall, Med. Phys. 17 (1990) 922–925.
[9] G. Jayaraman, K. Tiwari, Flow in a catheterized curved artery, Med. Biol. Eng. Comput. 33 (1995) 1–6.
[10] R.K. Dash, G. Jayaraman, K.N. Metha, Estimation of increased flow resistance in a narrow catheterized artery – A theoretical model, J. Biomech. 29 (1996) 917–930.
[11] R.K. Dash, G. Jayaraman, K.N. Metha, Flow in a catheterized curved artery with stenosis, J. Biomech. 32 (1999) 49–61.
[12] P. Daripa, R.K. Dash, A numerical study of pulsatile blood flow in an eccentric catheterized artery using a fast algorithms, J. Eng. Math. 42 (2002) 1–22.
[13] K. Vajravelu, S. Sreenadh, V. Ramesh Babu, Peristaltic transport of a Herschel–Bulkley fluid in an inclined tube, Int. J. Nonlinear Mech. 40 (2005) 83–90.
[14] D.S. Sankar, K. Hemalatha, Pulsatile flow of Herschel–Bulkley fluid through catheterized arteries – A mathematical model, Appl. Math. Model., in press, doi:10.1016/j.apm.2006.04.012.
[15] G.W. Scott Blair, D.C. Spanner, An Introduction to Biorheology, Elsevier Scientific Publishing Company, Amsterdam, 1974, p. 51.
[16] C. Tu, M. Deville, Pusatile flow of non-Newtonian fluids through arterial stenosis, J. Biomech. 29 (7) (1996) 899–908.
[17] N. Iida, Influence of plasma layer on steady blood flow in microvessels, Jpn. J. Appl. Phys. 17 (1978) 203–214.
[18] G.W. Scott Blair, The success of Casson equation, Rheol. Acta 5 (1966) 184–187.
[19] W.H. Leung, M.L. Stadius, E.L. Alderman, Determinants of normal coronary artery dimensions in humans, Circulation 84 (1991) 2294–2306.
[20] J.N. Kapur, Mathematical Models in Biology and Medicine, East-West Press Pvt. Ltd., New Delhi, India, 1992, pp. 368–369.
[21] P. Chaturani, R. Ponnalagar Samy, A study of non-Newtonian aspects of blood flow through stenosed arteries and its applications in arterial diseases, Biorheology 22 (1985) 521–531.
[22] E.W. Merrill, Rheology of human blood and some speculations on its role in vascular homeostasis, in: P.N. Sawyer (Ed.), Biomechanical Mechanisms in Vascular Homeostasis and Intravascular Thrombus, Appleton Century Crafts, New York, 1965.

[23] G. Cokelet, Biomechanics: its foundations and objections, in: Proceedings of a Symposium on Biomechanics, University of California, San Diego, Prentice-Hall, Englewood Cliff, NJ, 1970, pp. 29–31.
[24] E.L. Johnson, P.G. Yock, V.K. Hargrave, J.P. Srebro, S.M. Manubens, W. Seitz, T.A. Ports, Assessment of severity of coronary stenosis using a Doppler catheter. Validation of a method based on the continuity equation, Circulation 80 (1989) 625–635.
[25] P. Ganz, D.P. Harrington, J. Gaspar, W.H. Barry, Phasic pressure gradients across coronary and renal artery stenosis in humans, Am. Heart J. 106 (1983) 1399–1406.